International Journal of Nanomedicine

Dovepress
open access to scientific and medical research

Open Access Full Text Article

ORIGINAL RESEARCH

Combined Black Phosphorus Nanosheets with ICG/aPDT is an Effective Anti-Inflammatory Treatment for Periodontal Disorders

Xincong Li[1,*], Shuangshuang Ren[1,*], Lutong Song[1], Deao Gu[2], Haoran Peng[1], Yue Zhao[1], Chao Liu[2], Jie Yang[3], Leiying Miao[1]

[1]Department of Cariology and Endodontics, Nanjing Stomatological Hospital, Medical School of Nanjing University, Nanjing, Jiangsu, 210008, People's Republic of China; [2]Department of Orthodontics, Nanjing Stomatological Hospital, Medical School of Nanjing University, Nanjing, Jiangsu, 210008, People's Republic of China; [3]Department of Periodontology, Nanjing Stomatological Hospital, Medical School of Nanjing University, Nanjing, Jiangsu, 210008, People's Republic of China

*These authors contributed equally to this work

Correspondence: Leiying Miao; Jie Yang, Email miaoleiying80@163.com; dorothy0314@sina.com

Introduction: Antibacterial photodynamic treatment (aPDT) has indispensable significance as a means of treating periodontal disorders because of its extraordinary potential for killing pathogenic bacteria by generating an overpowering amount of reactive oxygen species (ROS). The elevated ROS that may result from the antibacterial treatment procedure, however, could exert oxidative pressure inside periodontal pockets, causing irreparable damage to surrounding tissue, an issue that has severely restricted its medicinal applications. Accordingly, herein, we report the use of black phosphorus nanosheets (BPNSs) that can eliminate the side effects of ROS-based aPDT as well as scavenge ROS to produce an antibacterial effect.

Methods: The antibacterial effect of ICG/aPDT was observed by direct microscopic colony counting. A microplate reader and confocal microscope enabled measurements of cell viability and the quantification of ROS fluorescence. BPNS administration regulated the oxidative environment. IL-1β, IL-6, TNF-α, IL-10, TGF-β, and Arg-1 mRNA expression levels were used to assess the inflammatory response after BPNS treatment. In vivo, the efficacy of the combination of BPNSs and ICG/aPDT was evaluated in rats with periodontal disease by histomorphometric and immunohistochemical analyses.

Results: The CFU assay results verified the antibacterial effect of ICG/aPDT treatment, and ROS fluorescence quantification by CLSM indicated the antioxidative ability of the BPNSs. IL-1β, IL-6, TNF-α, IL-10, TGF-β, and Arg-1 mRNA expression levels were significantly decreased after BPNS treatment, confirming the in vitro anti-inflammatory effect of this nanomaterial. The histomorphometric and immunohistochemical analyses showed that the levels of proinflammatory factors decreased, suggesting that the BPNSs had anti-inflammatory effects in vivo.

Conclusion: Treatment with antioxidative BPNSs gives new insights into future anti-inflammatory therapies for periodontal disease and other infection-related inflammatory illnesses and provides an approach to combat the flaws of aPDT.

Keywords: periodontitis, black phosphorus nanosheets, reactive oxygen species, antibacterial photodynamic therapy, macrophage polarization

Introduction

As a complicated immune response to bacterial plaque, periodontal disease typically results in immunosuppression, bacterial overgrowth, irreparable damage, and tooth loss.[1] By creating toxins and indirectly triggering the endogenous immune system,[2,3] large amounts of cytokines, including interleukin-1 beta (IL-1β), tumor necrosis factor-alpha (TNF-α) and interleukin-6 (IL-6), and other factors are released, resulting in localized periodontal tissue inflammation and ultimately the destruction of the tissue that supports the of teeth.[4,5]

Received: 7 November 2022
Accepted: 8 February 2023
Published: 15 February 2023

Graphical Abstract

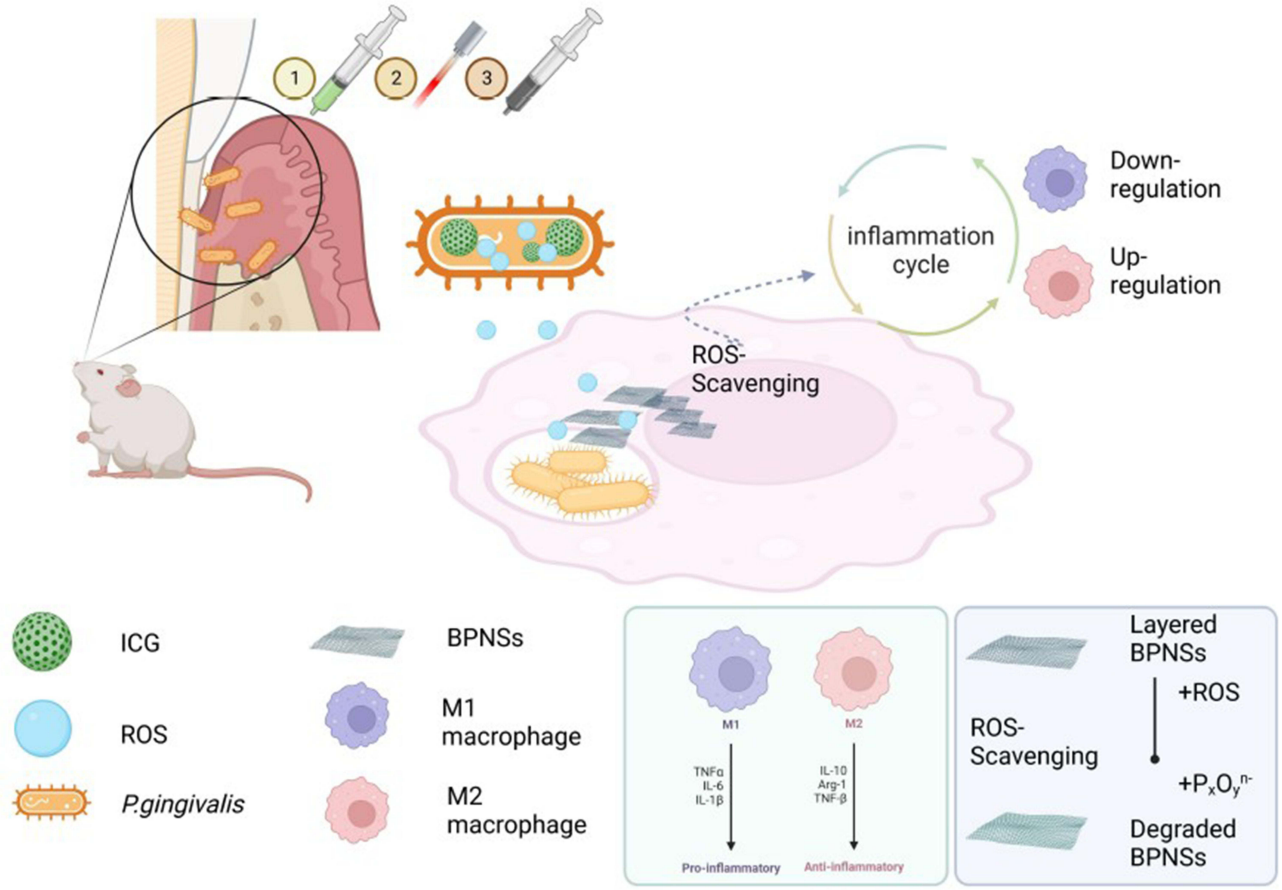

The use of aPDT for the treatment of bacterial illnesses, such as periodontitis, urinary tract infections, and burn wound infections, has grown significantly in recent years.[6] Photoactivatable photosensitizers used in aPDT can produce copious amounts of ROS instantly by photocatalysis after being exposed to laser excitation, which has the beneficial therapeutic effect of lowering the risk of the emergence of drug-resistant bacteria. Currently, mechanical debridement of the tooth surface is the primary method by which periodontitis and periodontal inflammation are treated.[7,8] However, this approach might promote bacterial aggregation because periodontal pockets are in the open environment of the oral cavity, and scaling and root planning frequently leave scratches on the tooth surface. The nonspecific bactericidal or bacteriostatic actions of antibiotics can inhibit both the bacteria and cells at the site of infection. aPDT has been proposed as an effective and specific antibacterial method because it enables the infiltration of photosensitizers into tissue. By rapidly releasing ROS after exposure to external light, aPDT has distinct benefits in periodontitis therapy compared with the mechanical method, as aPDT has a wide operating range and high efficiency and is easy to use.[9] Numerous recently published studies indicate that aPDT increases bacterial death and inhibits the release of virulence factors, exerting therapeutic benefits comparable to those of local antibiotic administration and increasing the therapeutic effects of clinical periodontitis treatment.[10,11]

ROS have two opposing effects in the human body. However, in regeneration research on periodontitis, the signs of ROS-induced inflammation in aPDT have been disregarded, which restricts its change from nonclinical use.[12] The destruction of microorganisms by aPDT relies upon the quick release of significant amounts of ROS,[13] which will increase the local concentration of unneeded ROS and introduce oxidative pressure in the tissues surrounding the teeth.

This could then allow the initiation of adverse endogenous cell immunity, which might then cause the degradation of proteins, nucleic acids, and other components and promote excessive inflammation, finally leading to cell death and tissue deterioration.[14,15] The imbalance in host oxidant/antioxidant regulation and the accumulated ROS after aPDT increase the risk of local inflammation of delicate tissue and accelerated bone loss in periodontal tissues. Consequently, inflammatory cells are drawn to the area, and macrophages are polarized to the M1 phenotype, both of which have a negative impact on periodontal tissue.[16,17] In this manner, in aPDT, ROS could kill bacteria but exacerbate the inflammatory response, which, to some extent, hinders advancement of the clinical applications of aPDT. Decreasing the generation and effects of ROS is the way to resolve this inconsistency.[18] To minimize excessive local oxidative pressure for the safe application of aPDT in periodontal illnesses, it is highly desirable to develop a unique aPDT treatment approach that can produce exceptional antibacterial effects that are quickly followed by ROS scavenging.

Black phosphorus nanosheets (BPNSs), as two-dimensional materials, have demonstrated extraordinary potential in biomedical applications. The physical parameters of BPNSs, such as their shape, size, electronics, and optical qualities, play significant roles in determining their potential.[26] In the phosphorus monolayer, each phosphorus atom is connected to three adjacent phosphorus atoms through covalent bonds to form a folded layered structure. This phosphorus layer and surface are in close proximity to each other due to van der Waals forces.[26] Compared with other 2D nanomaterials, nanoscale black phosphorus sheets have a folded, double-layer structure along the Z-axis. This folded structure gives the black phosphorus nanosheets a higher specific surface area and serves as the basis for the ROS scavenging effects. Quick electron transfer is made possible by the packed layer structure of the BPNSs, and their elemental state facilitates an easy and fast oxidative reaction to form P–O bonds, giving these nanomaterials a potent capacity to consume ROS.[24,25] The distinct physical shape of BPNSs, such as their flake-like framework, along with their strong ROS scavenging ability and low in vivo cytotoxicity, ensures that these BPNSs could effectively operate as antioxidants to eliminate ROS. Additionally, after providing protection, the BPNSs produce biocompatible, nontoxic $P_xO_y^{n-}$ ions as their end products.[19,20] These intriguing characteristics made BPNSs viable therapeutic candidates to reduce oxidative stress in conditions linked to ROS. BPNSs not only exhibit excellent antioxidant effects but can also be used to stimulate bone regeneration even under disease conditions, such as those involving tumors and infection. Thus, a multifunctional platform that can not only eliminate infection but also promote bone regeneration is strongly needed for the treatment of periodontal disease.[21–23]

Even though BPNSs are among the most bioactive nanomaterials and they exhibit exceptional chemical reactivity toward ROS, BPNSs have not yet been specifically studied in this regard.[22] There are currently no safe and effective candidates for antioxidative therapy, although the need to reduce oxidative pressure has long been understood.[20,21] Therefore, a research study on BPNSs as potent antioxidative agents for the treatment of periodontal inflammatory disease is needed. Herein, we demonstrated how BPNSs can protect against the harmful effects caused by excessive ROS during aPDT treatment of periodontal disease. This work presents a novel opportunity to develop BPNSs into new, proficient, antioxidative materials to fulfill the clinical need to treat ROS-related inflammatory diseases.

Materials and Methods

The Synthesis of Black Phosphorus Nanosheets

BPNSs with a large surface area were obtained through a liquid exfoliation technique. Ultrapure water (100 mL) was mixed with bulk black phosphorus (100 mg), and then N_2 was bubbled into the solution to remove any dissolved O_2. Liquid exfoliation of the bulk BP was then carried out by placing the mixture in an ultrasonicator (KQ-200KDE; 100% power, 8 h). To remove any nonexfoliated bulk BP, the solution was centrifuged at 2000 rpm for 5 minutes after the reaction. The BPNSs and colloids were separated by centrifuging the remaining supernatant at 12,000 rpm for 10 minutes.

Characterization of the Black Phosphorus Nanosheets

A laser Raman spectrometer (XPLORA INV) was used to scan 0.1 mL of distilled water containing 50 μg of BPNSs and 3 μg of H_2O_2 at 0, 2, and 5 min after 633 nm laser excitation. The ability of the BPNSs (46 μL, 10 to 110 μg/mL) to eliminate hydroxyl/superoxide anion radicals was evaluated using ESR spectroscopy (JEOL-FA200). UV–Vis

spectroscopy was used to measure the absorbance of pure solutions of •$ABTS^+$ radicals and •$ABTS^+$ radical solutions containing BPNSs at 734 nm. Based on the proportion of neutralized radicals to total radicals, the inhibition rate of •$ABTS^+$ radicals was estimated. All measurements were performed in triplicate.

Bacterial Culture for Antibacterial Experiment

Porphyromonas gingivalis (*P. gingivalis*, ATCC 33277) was obtained commercially from American Type Culture Collection (ATCC, Manassas, VA, USA) and cultured on Columbia blood agar plates in an anaerobic environment at 37 °C. A single colony was inoculated in 10 mL of brain heart infusion broth (B8130, Solarbio, China) supplemented with 5 mg/L hemin (H6390, Sigma–Aldrich, USA), 10 mg/mL vitamin K1 (V3501, Sigma–Aldrich, USA), and 50 mL/L sterile defibrinated sheep blood (R54020, ThermoFisher, USA). The bacterial suspensions were centrifuged after five days and then resuspended in phosphate-buffered saline (PBS, KeyGen, China).

Parameters of Photosensitizer in Photodynamic Experiment

ICG was obtained from TCI Development Co., Ltd. (No. 10,535, China). A laser diode module with a maximum absorption wavelength of 808 nm and a power of 1.65 W/cm^2 was employed. A current of up to 50 mA can be used to run this laser.

An ultraviolet–visible (UV–Vis) spectrophotometer (Shimadzu UV-2550, Japan) was used to examine the steady performance of ICG. Ten milliliters of PBS was added to 40 μg/mL ICG. One milliliter of the release medium was removed, and the UV–Vis absorption spectrum was acquired at predetermined intervals. ICG (0, 20, 40, 60 and 80 μg/mL) was dispersed in PBS, and real-time fluorescence images were obtained with the probe DCFH-DA. ICG was dispersed in PBS and irradiated with NIR light (1.65 W/cm^2, 808 nm) for 10 min. Temperature changes were recorded, and real-time infrared thermal pictures were taken using infrared thermal imaging (IRIS-500, Medicore, USA). Real-time fluorescence images were obtained with the DCFH-DA probe and observed by CLSM (A1R, Nikon, Japan). The fluorescence intensity was recorded every 30s.

In vitro Antibacterial Properties of Black Phosphorus Nanosheets

P. gingivalis suspensions (1.0× 10^8 CFU/mL, 180 μL) were coincubated in 96-well plates with the appropriate reagents to establish the following treatment groups: PBS, ICG, ICG/aPDT, ICG+BPNSs and ICG/aPDT+BPNSs. Then, NIR light irradiation or dark treatment was performed for 3 min according to the requirements of the different groups. After incubation for 1 h at 37 °C in 5% CO2 in the dark, the bacterial suspensions were collected, serially diluted to an appropriate concentration, and then plated onto LB agar plates for CFU counting.

Intracellular ROS Levels of Various Treatments

HGF-1 cells (ATCC: CRL2014) were cultured in confocal microscopy dishes and treated with various treatments (control, ICG, ICG/aPDT and ICG/aPDT+BPNSs) for 4 h. Then, the medium was replaced with fresh culture medium, and the cells were treated with/without 808 laser irradiation (1.65 W/cm^2) for 3 min. Cells were then exposed to the DCFH-DA probe for 20 min, washed three times and examined by CLSM.

In vitro Cytotoxicity of Black Phosphorus Nanosheets

In vitro cytotoxicity was assessed by a CCK-8 assay kit obtained from Abcam (ab228554, England). HGF-1 cells were plated in 96-well plates (5× 10^3 cells/well) and grown overnight to reach 80% confluence. Then, cells were treated with ICG (20, 40, 60 and 80 μg/mL; 50 μL) for 24 h. After 4 hours of incubation, the cells in the ICG groups were treated with or without BPNSs (200 μg/mL, 50 μL) and irradiated at 808 nm (1.65 W/cm2, 3 min). Then, new culture medium containing CCK-8 was added. After incubation for 4 h, the absorbance was measured with a microplate reader at 460 nm.

After various treatments, the cells were stained with FDA/PI (BES20118BO, BIOESN, China) and observed by CLSM to evaluate cytocompatibility.

Anti-Inflammatory Properties of Black Phosphorus Nanosheets Against Pro-Inflammatory aPDT Induced

RAW 264.7 cells (ATCC TIB71, Thermo Fisher Scientific) were plated at a density of 2.5×10^5 cells/well and cultivated for 24 hours. The nonirradiated groups containing BPNSs were utilized to compare the anti-inflammatory efficacy of the BPNSs against periodontal diseases. Comparative research into the ability of BPNSs to prevent aPDT-aggravated inflammation during periodontal disorder treatment was conducted using groups of ICG/aPDT+BPNSs.

IL-1β, IL-6, TNF-α, IL-10, TGF-β, and Arg-1 mRNA expression levels were used to assess the inflammatory response of cells with the M1/M2 phenotype. Each sample was run in duplicate, and each experiment was conducted three times. Table 1 lists the primer sequences for each cytokine.

In vivo Therapeutic Efficacy

Twenty-five Sprague–Dawley rats (6 weeks old, male, 160–180 g) were obtained from Vital River Laboratories (Beijing, China). All animals were kept in an environment with a constant humidity and temperature. The Nanjing University Institutional Animal Care and Use Committee authorized all procedures involving animals (IACUC-2003040).

SD rats were fed for seven days to adapt to the environment and then randomly divided into five groups: control group, ICG group, ICG/aPDT group, ICG+BPNS group and ICG/aPDT+BPNS group {ICG (1 mg/mL, 100 μL), BPNSs (20 μL/mL, 200 μL), NIR (808 nm laser, 1.65 W/cm^2, 3 min of irradiation per day)}. *P. gingivalis* LPS (60 μg/mL, 100 μL) and mixed bacteria (*P. gingivalis*, 10^8 CFU/mL, 100 μL) were injected into the palatal gingivae under the second maxillary molar every day. Then, ICG was injected and 808 nm laser irradiation was applied in situ for 3 min per day for a total of 3 days of modeling. BPNSs were administered in situ at a dose of 200 μL per rat. Five specimens were anesthetized by inhalation of isoflurane (2% in 100% oxygen), and the organs were harvested postoperatively at 1 week for histological observation.

Histomorphometry and Immunohistochemical Analyses

Hematoxylin and eosin (H&E) was used to stain each slide. A light microscope (Olympus) was used to view the H&E-stained slides. At 200× magnification, inflammatory regions were visible, and at 400× magnification, the immune cells could be counted.

Immunohistochemical (IHC) staining was utilized to gauge the levels of proinflammatory cytokines in the tissue that had been removed. Rabbit anti-TNF-α (ab6671, Abcam), rabbit anti-IL-6 (ab7737, Abcam) and rabbit anti-IL-1β (ab9722, Abcam) were used as primary antibodies. Under a light microscope, images were seen and recorded (Olympus). For each group, ImageJ was used to randomly count the number of cells positive for each protein at a high magnification.

Statistical Analysis

The data are presented as the means ± standard deviations. Statistical analyses were performed with GraphPad Prism 8. To determine the significance of the variables, one-way analyses of variance (ANOVA) were carried out. ***$p < 0.001$ indicates statistical significance.

Table 1 Primer Sequences

Gene	Forward Sequence (5′ to 3′)	Reverse Sequence (3′ to 5′)
IL-1β	GAAATGCCACCTTTTGACAGTG	TGGATGCTCTCATCAGGACAG
IL-6	CTTCTTGGGACTGATGCTGGT	CACAACTCTTTTCTCATTTCCACG
TNF-α	CAGGCGGTGCCTATGTCTC	CGATCACCCCGAAGTTCAGTAG
TGF-β	CTTCAGCCTCCACAGAGAAGAACT	TGTGTCCAGGCTCCAAATATAG
Arg-1	ACACGGCAGTGGCTTTAACC	GGCGTTTGCTTAGTTCTGTCTG
IL-10	TACGGCGCTGTCATCGATTT	TAGAGTCGCCACCCTGATGT

Results and Discussion

ICG/aPDT-Mediated Intracellular ROS Production

The impacts of various concentrations of indocyanine green (ICG), an optical imaging agent with NIR fluorescence at 780 nm, on aPDT were determined (Figure 1A). Photoinactivation was found to be dose-dependent (Figure 1B). The ROS level increased with the ICG concentration. In addition, after ICG absorbs the energy from the laser, the majority of the energy is converted into nuclear power as the main ICG energy transformation. With increasing ICG concentration and irradiation time of the laser, the thermal impact becomes more obvious. In general, when tissues of the body reach a temperature of 41.5 °C, cytotoxicity appears, an effect that increases when the temperature reaches 43 °C (Figure 1C). In this study, we did not want to damage the surrounding tissues, so it was not necessary to create high temperatures (greater than 43 °C); thus, 60 and 80 μg/mL ICG were not the optimal choices. HGF-1 cells exposed to 20 and 40 μg/mL ICG and irradiation showed no discernible differences compared to the control group ($P>0.05$). However, the degree of cell survival began to decline at an ICG concentration of 60 μg/mL ($P<0.05$), and this decline continued at the higher ICG concentration (80 μg/mL), as shown in Figure 1D. The level of ROS rose during the initial 180 s when irradiated and treated with 40 μg/mL ICG, but this level did not increase after 180 s, demonstrating the ability of ICG to quickly absorb the light and produce a large amount of ROS within 180 s (Figure 1E and F). Combining the above data, it can be concluded that 40 μg/mL ICG and 808 nm of NIR irradiation for 3 min were the optimal experimental conditions.

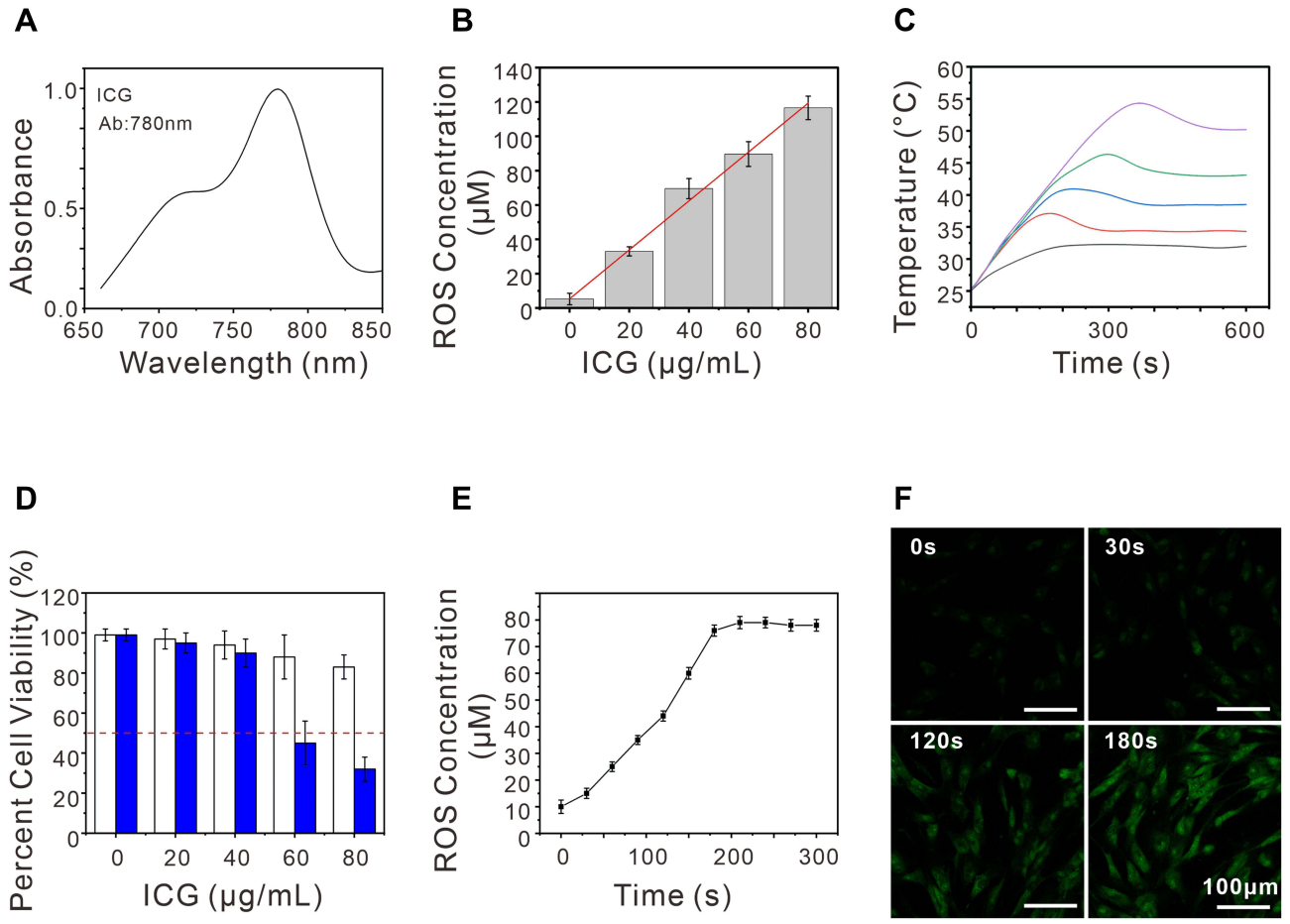

Figure 1 The total and intracellular ROS generation via ICG/aPDT. (**A**) UV-vis absorption spectra of ICG; (**B**) ROS production dynamics for different ICG concentrations under 808 nm laser irradiation; (**C**) Temperature variation curves of the ICG solution under different concentrations after treatment with 808 nm laser irradiation (40 μg/mL ICG, 1.65 W/cm^2, from 0 to 10 min); (**D**) Cell viability after treatment with various ICG doses with or without 808nm laser irradiation; (**E**) ROS production curve converting 0 to 5 min; (**F**) Fluorescence intensity of DCF via different times.

Antibacterial Properties of ICG/aPDT

Porphyromonas gingivalis (*P. gingivalis*, ATCC 33277) was chosen as a representative periodontal pathogen for in vitro antibacterial evaluation since it is crucial to the development and progression of periodontitis.[27] As displayed in Figure 2A and B, the inhibitory effect induced by 40 μg/mL ICG appeared rapidly and peaked after 180 s. As

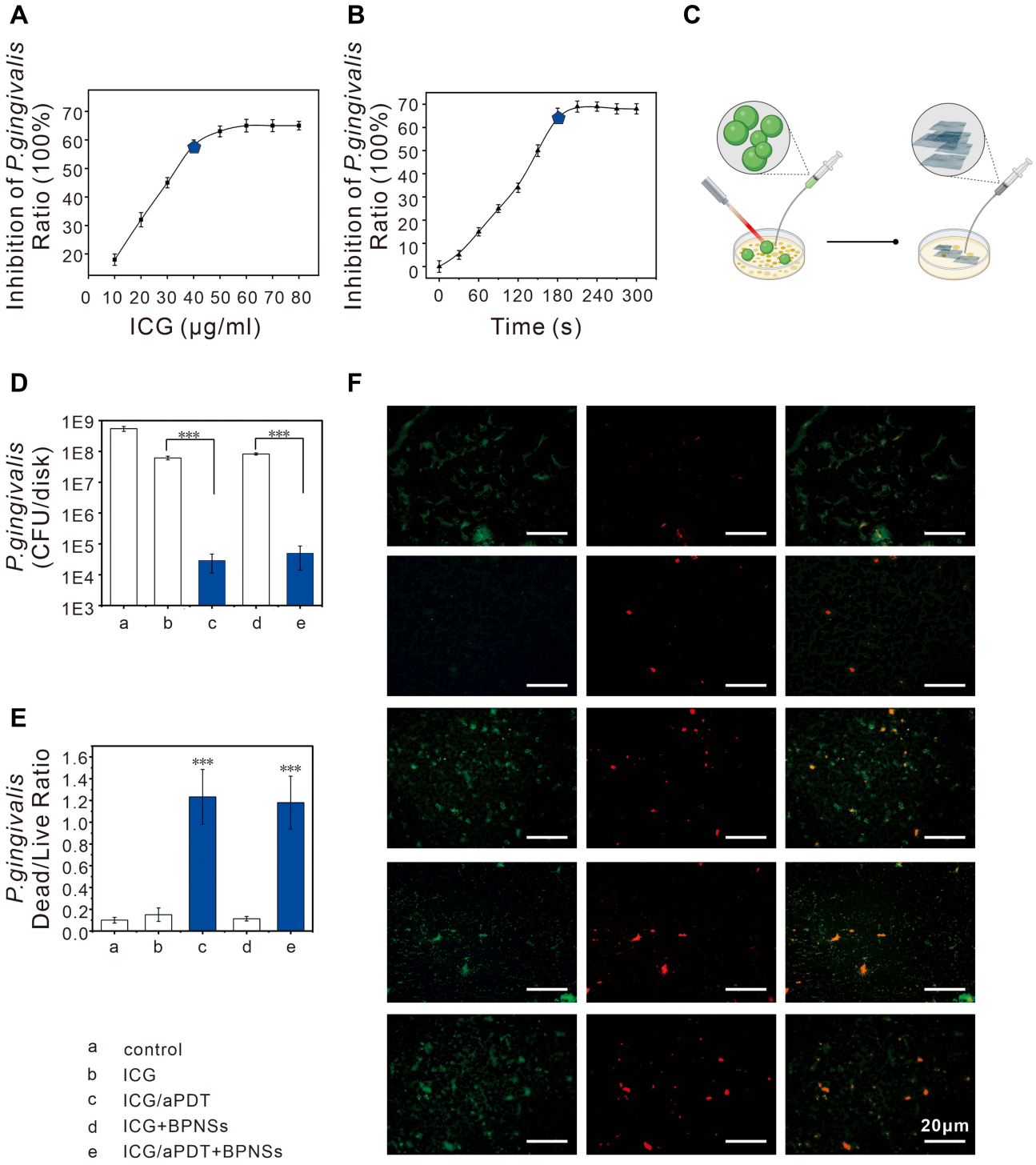

Figure 2 Antibacterial properties of ICG/aPDT. (**A**) Inhibition of *P. gingivalis* ratio with different ICG concentrations; (**B**) Inhibition of *P. gingivalis* ratio with different times (ICG, 40μg/mL); (**C**) A flow diagram for an antimicrobial experiment; (**D**) CFU counts of *P. gingivalis* with different treatments; (**E**) Dead/ live bacteria ratio for *P. gingivalis*; (**F**) Dead/live images of *P. gingivalis* with different treatments; (n = 3, ***$P < 0.001$).

a result, in the trials that followed, *P. gingivalis* was incubated with ICG for 180 s before being exposed to laser light. We then carried out the experiments as shown in the diagram in Figure 2C. Simple colony counting was used to determine the ratios of dead bacteria following the various treatments (Figure 2D). Surviving bacteria were colored green with FDA after utilizing a live/dead viability staining technique and observing by CLSM. Figure 2F shows bacteria with damaged cell membranes stained red by PI. Statistical analysis of the fluorescence data are shown in Figure 2E. Almost all of the bacteria in the control group survived, as observed by the green fluorescence. Only a few red-stained cells were present in the ICG group and ICG+BPNS group compared to the control group, indicating that with or without BPNSs, ICG at a concentration of 40 μg/mL exhibited a slight bactericidal effect. However, most of the bacteria in the ICG/aPDT group displayed red fluorescence, demonstrating that after photodynamic bactericidal treatment, a large percentage of the microbes had been eradicated. In addition, BPNSs did not weaken the antibacterial effect of ICG/aPDT.

Systematic ROS Scavenging Capacity of Black Phosphorus Nanosheets

The ability of the BPNSs to scavenge ROS was examined in light of the critical function of ROS in periodontitis. H_2O_2, •OH, and $O_2^{\bullet-}$ were chosen to evaluate the capacity of the BPNSs to scavenge multiple kinds of ROS. As shown in Figure 3, the morphology of the layered BPNSs was characterized by TEM (Figure 3B), and the nanomaterials had an average lateral dimension of 220±15.0 nm by DLS (Figure 3A). The ABTS radical cation decolorization assay was used to measure the antioxidative effectiveness, and the BPNSs eliminated virtually all of the •ABTS+ radicals within 120 s (Figure 3C). The capacity of the BPNSs to scavenge H_2O_2 was evaluated using Raman spectroscopy (Figure 3D). Because the BPNSs exhibit peaks at approximately 358, 434, and 460 cm^{-1} and H_2O_2 produces a strong Raman signal at approximately 897 cm^{-1}, we were able to recognize the reaction between the BPNSs and H_2O_2. The BPNS Raman peaks

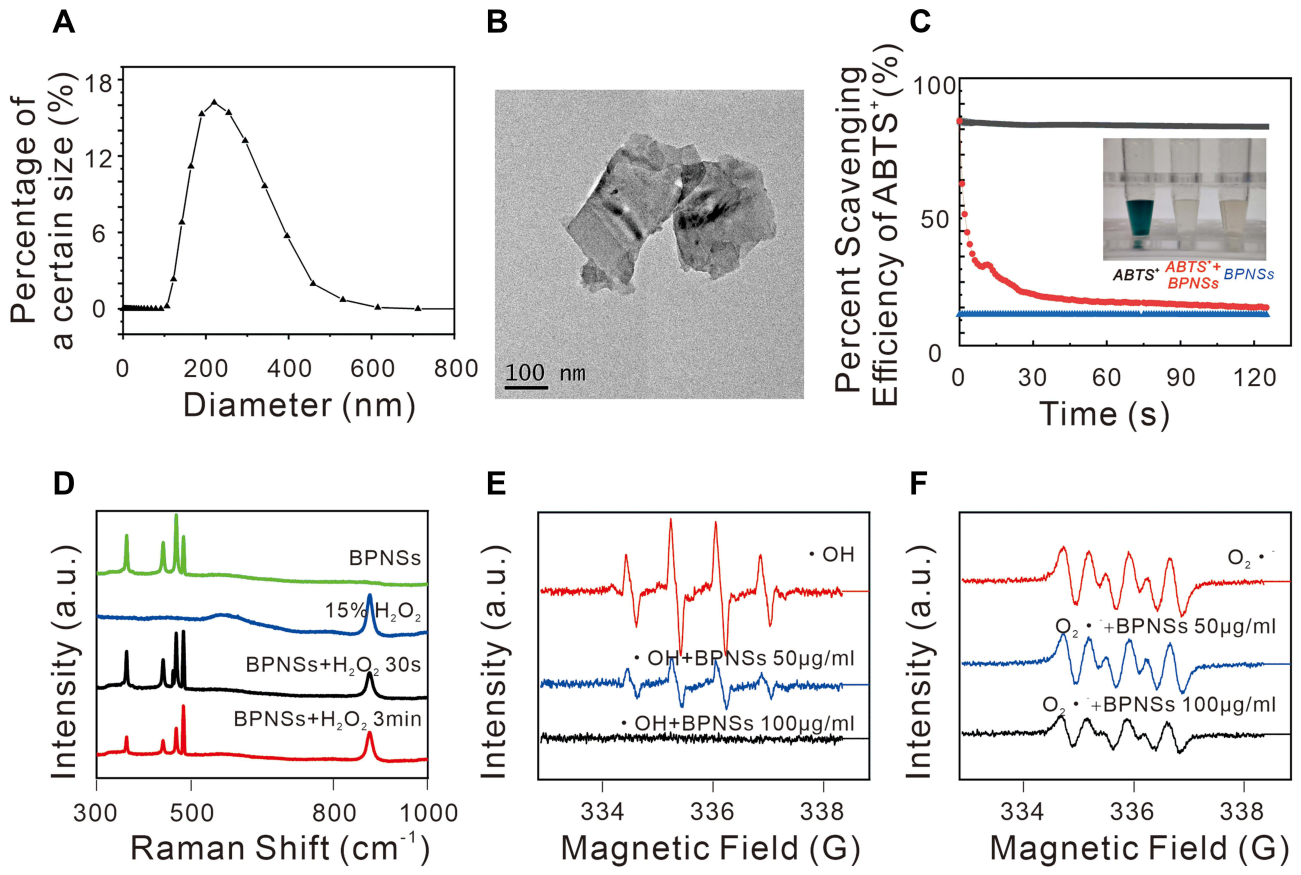

Figure 3 The morphology and systematic performance of BPNSs in terms of ROS scavenging. (**A**) DLS analysis of BPNSs; (**B**) TEM images of BPNSs; (**C**) The ABTS radical cation decolorization assay, with digital images of scavenging ABTS radicals. (line black: •$ABTS^+$; line red: •$ABTS^+$+ BPNSs; line blue: BPNSs); (**D**) Raman spectra of BPNSs reacted with H_2O_2; (**E**) •OH scavenging efficiency of BPNSs; (**F**) $O_2^{\bullet-}$ scavenging efficiency of BPNSs.

gradually decreased after both the addition of H_2O_2 and the lengthening of the incubation time. The free radical scavenging capability of the BPNSs was evaluated based on the reduction of $•ABTS^+$ radicals using an ABTS radical cation decolorization assay. The kinetics of the reaction with H_2O_2 were fast and H_2O_2 consumption was complete within 3 min, suggesting the high intracellular antioxidant activity of the BPNSs given that H_2O_2 is one of the main generators of cellular ROS. Therefore, among antioxidative nanomedicines, BPNSs could be used as novel treatment for quick and effective ROS scavenging. Additionally, the Fenton reaction generated hydroxyl radicals (•OH), which were visible as multiple peaks in a 1:2:2:1 ratio by electron spin resonance (ESR) spectroscopy. When BPNSs were added to the samples, the •OH peaks in the ESR spectrum dramatically diminished (Figure 3E). Superoxide anion radicals were produced by irradiating a solution of riboflavin. $O_2^{•-}$ underwent photodecomposition, and its ESR signal also gradually decreased with the addition of BPNSs (Figure 3F). The variations in the relative peak intensities in the ESR spectra of the DMPO− •OH/DMPO−$O_2^{•-}$ adducts pointed to the ROS scavenging activity of the BPNSs.

The subatomic architecture of the BPNSs serves as the foundation for their ROS scavenging mechanism.[26] BPNSs, a type of basic phosphorus, are composed of black phosphorus held together by weak van der Waals forces and have outstanding synthetic relevance for particles. The BPNSs' layer-pressed architecture facilitates rapid electron transfer, and their simple natural state provides a prompt oxidative response to form P–O bonds, revealing their powerful capacity to scavenge ROS.

Black Phosphorus Nanosheets Protect Cells from ROS Damage

In general, we believe that bacterial colonization after basic periodontitis treatment is the main reason for recurrent disease. By utilizing a large amount of ROS in a short amount of time, aPDT could purposefully and effectively kill bacteria. However, excessive ROS increases the burden of immune cells, including neutrophils and monocytes, at infected sites. As a result, it is essential to discover a biologically safe antioxidant that can effectively eliminate excess ROS and restore a microenvironment favorable for immune cell survival. In earlier research, aPDT destroyed bacteria by producing ROS.[28,29] In comparison to ICG alone, ICG under 808 nm laser irradiation showed increased antibacterial efficacy. Theoretically, when BPNSs are combined with ICG/aPDT, the ROS formed by ICG/aPDT would be countered by the ROS scavenging antioxidant activities of the BPNSs, maintain the antibacterial capabilities of aPDT.

We also investigated how BPNSs protect cells from ROS damage. The fluorescent dye DCF, which can be oxidized by intracellular ROS to produce green fluorescence, served as a marker for the presence of ROS. First, the CCK-8 cytotoxicity test was used to assess cell viability when different BPNS doses were applied. As displayed in Figure 4A, BPNSs initiated nominal cytotoxicity at concentrations ranging from 100 to 400 μg/mL. The favorable in vitro ability of the BPNSs to protect against ROS was demonstrated by the fact that the intensity of DCF after the addition of BPNSs significantly decreased in comparison to that in the ICG/aPDT group. The DCF fluorescence intensity was higher in the ICG/aPDT group than in the control group, highlighting the increased intracellular ROS in this treatment group. In Figure 4B and C, the confocal images and associated analyses of the fluorescently stained *P. gingivalis* treated with ICG/aPDT+BPNSs showed the scavenging of ROS by the BPNSs. The green fluorescence intensity was highest in the ICG/aPDT group because the DCF probe displayed green fluorescence in the presence of ROS. After cotreatment with BPNSs, the green fluorescence signal was severely reduced. The quantified data in Figure 4B demonstrate the same trend as that in the confocal images. Therefore, BPNSs may significantly reduce the intracellular ROS content.

Macrophages are quite important, as they are the most basic regulators of various natural cycles.[29] Depending on the pathophysiologic circumstance, such as that in periodontal disorders, macrophages may behave differently.[30] M1 macrophages accumulate at the periodontal infection site in response to microorganism stimulation and serve as the body's natural immune system. M1 macrophages do this through a variety of mechanisms, including the release of cytokines and the generation of ROS in the mitochondria, which would surely and irreparably injure the tissues in the immediate vicinity. M2 macrophages, on the other hand, utilize oxidative mechanisms for longer-term tasks related to tissue repair and wound healing. Therefore, one of the key strategies to treat periodontal diseases is to reduce local irritation and restore the regenerative capacity of the encompassing tissues by the interconversion of M1 and M2 macrophages to regulate endogenous cellular immunity.

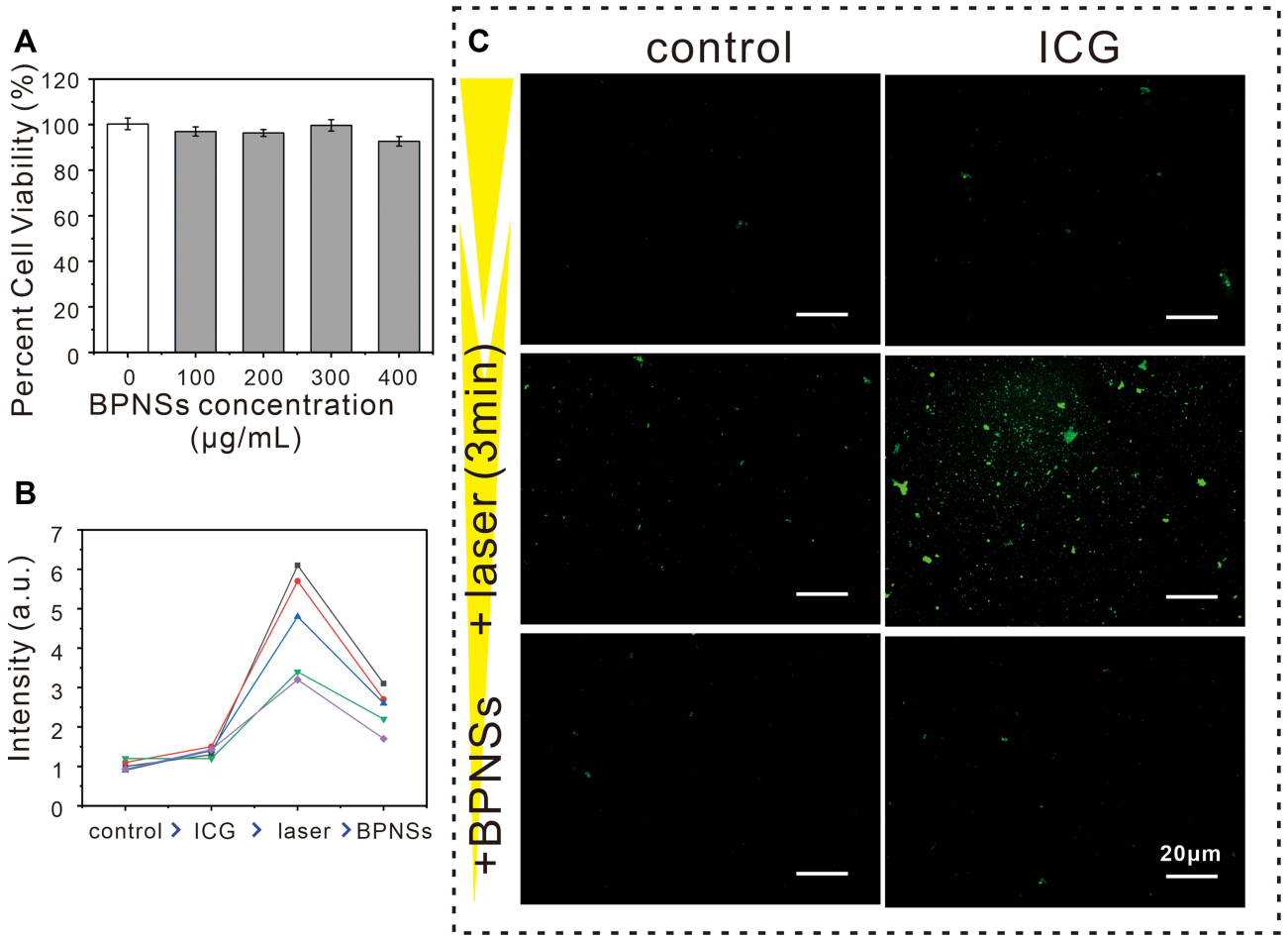

Figure 4 BPNSs' cellular protection against ROS damage. (**A**) Cell viability of HGF-1 cells treated with BPNSs at different concentrations; (**B**) Quantification analysis of DCF fluorescence intensity from confocal images; (**C**) Confocal images of the protective effect of BPNSs against ROS.

Effects of Black Phosphorus Nanosheets Against Inflammation Induced by ROS After ICG/aPDT

P. g-LPS was originally employed to mimic the inflammatory milieu to study the immunoregulatory effects of BPNSs on the inflammatory response, from the inflammation worsened by aPDT to the polarization of macrophages. The levels of cytokines related to inflammation were examined in M1 and M2 macrophages and RAW 264.7 cells. *P. g*-LPS was chosen to trigger inflammation and recreate the conditions of periodontitis to confirm the effects of the BPNSs on the alleviation of aPDT-aggravated inflammation. The levels of proinflammatory cytokines, such as IL-1β, TNF-α and IL-6, indicated that a significant number of macrophages were generated in response to *P. g*-LPS, as shown in the control group in Figure 5. Due to the increased generation of ROS compared to the control group, ICG/aPDT upregulated the expression of these proinflammatory factors. Such an escalation in proinflammatory molecules could potentially result in extensive tissue damage, accelerating the failure of the periodontium. Fortunately, ICG/aPDT+BPNS did not increase the contents of M1 macrophages, which were maintained the same level as that in the BPNS treatment groups. Due to the inherent antioxidative ability of BPNSs, these nanomaterials may be able to scavenge the very large amounts of ROS that are produced during the aPDT, resulting in decreased intracellular toxicity and the downregulation of M1-related factors. Intriguingly, the findings here also showed that BPNSs might polarize macrophages to change from the M1 phenotype to the M2 phenotype by increasing the expression levels of anti-inflammatory cytokine genes, including those for IL-10, Arg-1 and TGF-β. Figure 5 shows that compared to the control group, the ICG/aPDT group had increased mRNA levels of M1 markers and decreased expression levels of M2 markers. On the other hand, all of the BPNS-treated groups

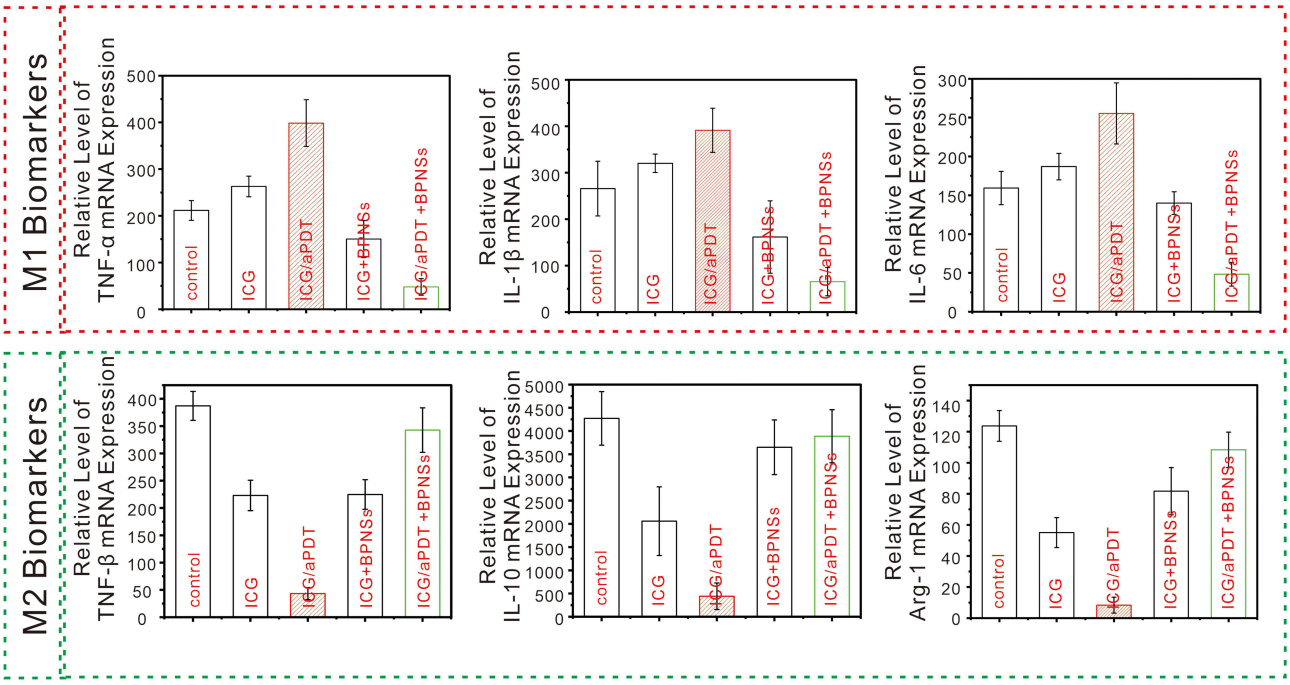

Figure 5 Anti-inflammatory response against BPNS inflammation caused by ICG/aPDT-aggravated ROS. Pro-inflammatory and anti-inflammatory gene expression is increased after being stimulated for three hours with *P. gingivalis*-LPS (1 μg/mL) for 3 h. (n = 3, $P < 0.05$).

demonstrated the ability to facilitate the transition from the M1 phenotype to the M2 phenotype by upregulating M2 marker expression due to the anti-inflammatory and wound-healing abilities of the BPNSs.

Overall, the results demonstrated the extraordinary and expected applicability of the use of BPNSs during aPDT-mediated periodontitis treatment. The administration of BPNSs results in fewer side effects and ultimately speeds up the immune response to prevent the dysregulation of tissue repair. BPNSs not only protect against ROS-induced oxidative damage but also polarize proinflammatory M1 macrophages into anti-inflammatory M2 macrophages.

In vivo Assessment of the Ability of Black Phosphorus Nanosheets to Suppress Periodontal Inflammation Aggravated by aPDT

Our in vivo study design is presented in Figure 1A. As shown in Figure 6B and C, inflammatory mediators were expressed and pathological alterations were observed in the area of the gingival tissue. The gingival tissues in the ICG group and the ICG/aPDT group were severely inflamed, as seen by the significant influx of inflammatory cells, including neutrophils and macrophages, as well as the loss of the gingival epithelium and lamina propria. In the ICG+BPNS group, concentrated inflammatory foci were seen, lymphocytes were the primary infiltrating cells, and the arteries were visibly hyperplastic, all of which pointed to a chronic inflammatory state. In the ICG/aPDT+BPNS group, compared with the ICG group and the ICG/aPDT group, the fibers were improved and fewer inflammatory cells were observed. H&E staining displayed a trend similar to that shown in Figure 6C. As shown in Figure 6D–F, compared with the control group, IHC staining of M1 polarization markers validated the significant reduction in M1-positive cells found in the ICG/aPDT group. In terms of the locations of inflammation, *P. g*- LPS and mixed *P. g* stimulation further increased the protein expression levels of M1 macrophage-specific indicators such IL-1β, IL-6 and TNF-α, while BPNS therapy significantly downregulated their expression.

The combination of *P. g*-LPS and *P. g* stimulated the inflammatory response and delivered toxic substances to cause periodontal disorders in the animal model. The ICG/aPDT group was successful in eliminating the local *P. g*; however, aPDT's antibacterial effects can also trigger inflammation, which limits its use in infectious disorders. Notably, ICG/aPDT+BPNS therapy induced efficient aPDT by lowering the inflammatory stimulus that the bacteria received from the

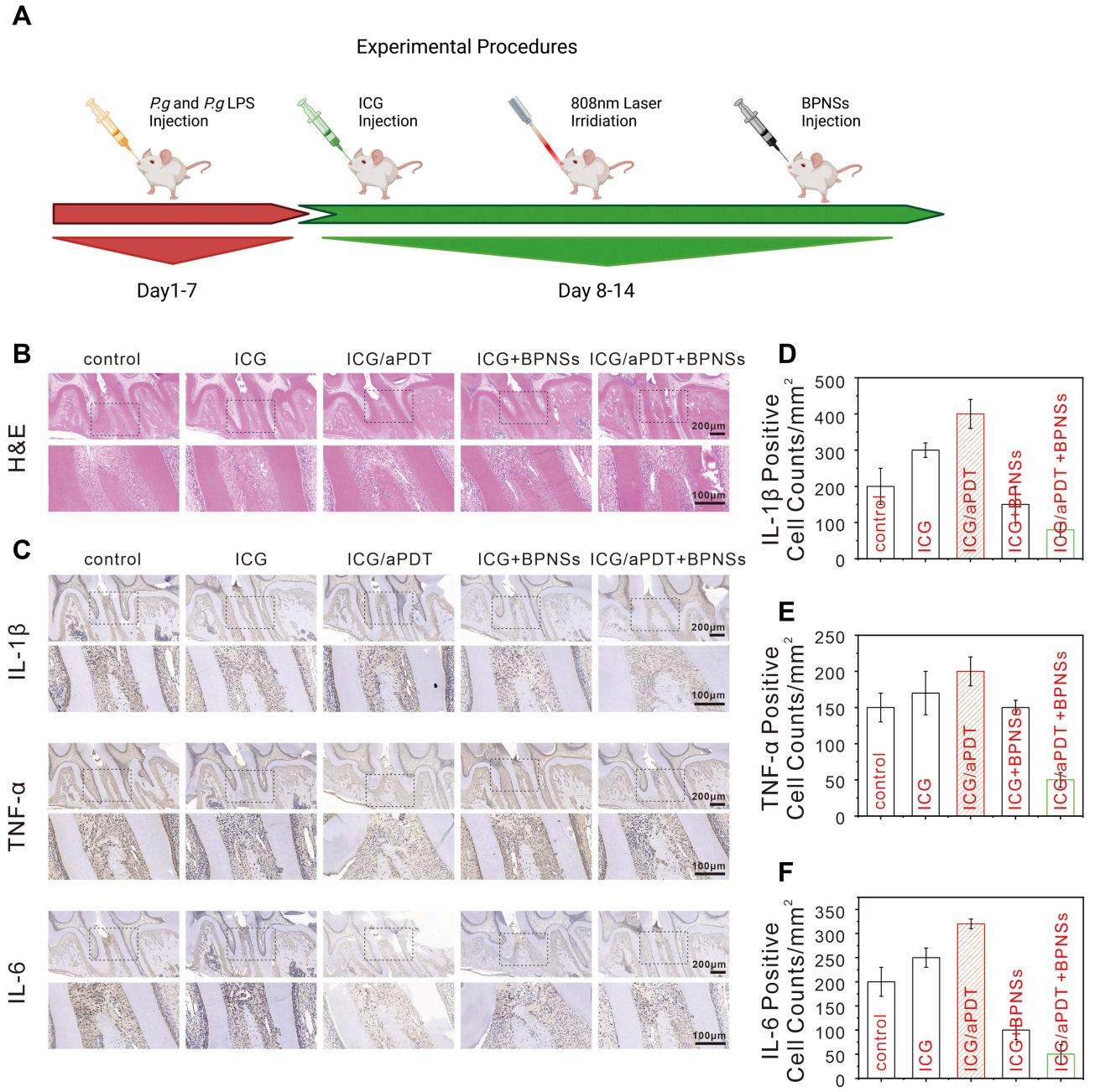

Figure 6 In vivo assessments of BPNSs on the suppression of aPDT-aggravated periodontal inflammation. An analysis of the pathological aspects of periodontal inflammation model triggered by *P. g*-LPS and *P. g*. (**A**) A flowchart of the in vivo tests, which includes medication administration and animal modeling. (**B**) H&E and (**C**) IHC assessment of periodontal tissues following treatments. (**D**–**F**) The equivalent measurement of positive cells with (**D**) IL-1β, (**E**) TNF-α and (**F**) IL-6 immunostaining.

environment. In addition, cotreatment with BPNSs lessened the negative effects of aPDT by reducing local inflammation by decreasing inflammatory mediator release and upregulating the expression levels of M2 markers with enhanced regeneration potential. These encouraging in vivo findings suggested that cotreatment with BPNSs would increase the use of aPDT in infectious disorders and offer outstanding potential for clinical periodontal disease therapy in the future.

Conclusions

In summary, the benefit of using BPNSs, which show a strong capacity to consume ROS, caused ICG/aPDT+BPNS treatment to have a unique capacity to solve the most troublesome issue confronting the clinical utilization of aPDT,

which is the contradiction of utilizing ROS for sterilization, as an excess of ROS leads to inflammation. This sequential therapy appropriately balances the antibacterial and anti-inflammatory activities by sensibly and viably adjusting the level of during and after aPDT. In addition to its antibacterial and anti-inflammatory effects, BPNS therapy shields healthy cells from the oxidative stress caused by aPDT and the subsequent inflammatory response. Our strategy of combining aPDT with the administration of antioxidative BPNSs can overcome the common flaws of aPDT simultaneously, which are tissue injury and poor ROS scavenging antibacterial activity. Thus, this approach of integrating antioxidants and aPDT would be very useful to fight infectious disorders, especially by managing tissue homeostasis in periodontitis.

Abbreviations

aPDT, antibacterial photodynamic treatment; ROS, receptive oxygen species; BPNSs, black phosphorus nanosheets; ICG, indocyanine green; FDA, fluorescein diacetate; PI, propidium iodide; DCFH-DA, 2′,7′-dichlorofluorescein diacetate; DLS, dynamic light scattering; ESR, electron spin resonance; UV-Vis, ultraviolet-visible; HGF-1 cells, human gingival fibroblast cells; *P.g, P.gingivalis*; LPS, lipopolysaccharide; qPCR, quantitative real time polymerase chain reaction; TNF-α, tumor necrosis factor-alpha; IL-1β, interleukin-1 beta; IL-6, interleukin-6; IL-10, interleukin-10; TGF-β, transforming growth factor-β; Arg-1, arginine-; SD rat, Sprague–Dawley rat; TEM, transmission electron microscopy; CLSM, confocal laser scanning microscopy; H&E, hematoxylin and eosin; IHC, immunohistochemical staining.

Ethics Approval

Sprague-Dawley rats (6-week-old, male, 160–180 g, certificate no. SCXK- (Zhejiang) 2019-0001) were obtained from Vital River Laboratories (Zhejiang, China). All animal experiments were performed under protocols approved by the Institutional Animal Care and Use Committee of the Nanjing University (IACUC-2003040). Moreover, approval was received prior to beginning this research.

Data Sharing Statement

The datasets used and/or analyzed during the current study are available from the corresponding authors on reasonable request.

Author Contributions

All authors made a significant contribution to the work reported, whether that is in the conception, study design, execution, acquisition of data, analysis and interpretation, or in all these areas; took part in drafting, revising or critically reviewing the article; gave final approval of the version to be published; have agreed on the journal to which the article has been submitted; and agree to be accountable for all aspects of the work.

Funding

This work was supported by the Natural Science Foundation of Jiangsu Province (Grant No. BK 20200665, BK20221177, SKB2022020532), Key Laboratory in Science and Technology Development Foundation, Nanjing Department of Health (Grant No. ZKX19031, ZKX22055), Nanjing Clinical Research Center for Oral Diseases (No.2019060009), and "2015" Cultivation Program for Reserve Talents for Academic Leaders of Nanjing Stomatological School, Medical School of Nanjing University (No.0223A203).

Disclosure

The authors declare that they have no conflicts of interest in this work.

References

1. Li X, Hu L, Ma L, et al. Severe periodontitis may influence cementum and dental pulp through inflammation, oxidative stress, and apoptosis. *J Periodontol*. 2019;90(11):1297–1306. doi:10.1002/JPER.18-0604

2. Kugaji MS, Kumbar VM, Peram MR, Patil S, Bhat KG, Diwan PV. Effect of Resveratrol on biofilm formation and virulence factor gene expression of Porphyromonas gingivalis in periodontal disease. *APMIS*. 2019;127(4):187–195. doi:10.1111/apm.12930
3. Sheets SM, Robles-Price AG, McKenzie RM, Casiano CA, Fletcher HM. Gingipain-dependent interactions with the host are important for survival of Porphyromonas gingivalis. *Front Biosci*. 2008;13:3215–3238. doi:10.2741/2922
4. Zhang J, Liang H, Zheng Y, et al. Photodynamic therapy versus systemic antibiotic for the treatment of periodontitis in a rat model. *J Periodontol*. 2019;90(7):798–807. doi:10.1002/JPER.18-0305
5. Wang H, Wang S, Cheng L, et al. Novel dental composite with capability to suppress cariogenic species and promote non-cariogenic species in oral biofilms. *Mater Sci Eng C Mater Biol Appl*. 2019;94:587–596. doi:10.1016/j.msec.2018.10.004
6. Campu A, Focsan M, Lerouge F, et al. ICG-loaded gold nanobipyramids with NIR activatable dual PTT-PDT therapeutic potential in melanoma cells. *Colloids Surf B Biointerfaces*. 2020;194:111213. doi:10.1016/j.colsurfb.2020.111213
7. Sobotta L, Skupin-Mrugalska P, Piskorz J, Mielcarek J. Porphyrinoid photosensitizers mediated photodynamic inactivation against bacteria. *Eur J Med Chem*. 2019;175:72–106. doi:10.1016/j.ejmech.2019.04.057
8. Yang X, Wang D, Shi Y, et al. Black phosphorus nanosheets immobilizing Ce6 for imaging-guided photothermal/photodynamic cancer therapy. *ACS Appl Mater Interfaces*. 2018;10(15):12431–12440. doi:10.1021/acsami.8b00276
9. Terra-Garcia M, de Souza CM, Ferreira Gonçalves NM, et al. Antimicrobial effects of photodynamic therapy with Fotoenticine on Streptococcus mutans isolated from dental caries. *Photodiagnosis Photodyn Ther*. 2021;34:102303. doi:10.1016/j.pdpdt.2021.102303
10. Qi M, Li X, Sun X, et al. Novel nanotechnology and near-infrared photodynamic therapy to kill periodontitis-related biofilm pathogens and protect the periodontium. *Dent Mater*. 2019;35(11):1665–1681.
11. Li W, Zhang H, Guo X, et al. Indocyanine green as a synchronous photodynamic-photothermal therapy platform that inhibits tumor growth and metastasis. *ACS Appl Mater Interfaces*. 2017;9(4):3354–3367. doi:10.1021/acsami.6b13351
12. Kishore A, Petrek M. Roles of macrophage polarization and macrophage-derived miRNAs in pulmonary fibrosis. *Front Immunol*. 2021;12:678457. doi:10.3389/fimmu.2021.678457
13. Griffiths HR, Gao D, Pararasa C. Redox regulation in metabolic programming and inflammation. *Redox Biol*. 2017;12:50–57. doi:10.1016/j.redox.2017.01.023
14. Gao Q, Zhang J, Chen C, et al. In situ mannosylated nanotrinity-mediated macrophage remodeling combats candida albicans infection. *ACS Nano*. 2020;14(4):3980–3990. doi:10.1021/acsnano.9b07896
15. Zhou J, Liu L, Wu P, Zhao L, Wu Y. Fusobacterium nucleatum Accelerates Atherosclerosis via Macrophage-Driven Aberrant Proinflammatory Response and Lipid Metabolism. *Front Microbiol*. 2022;13:798685. doi:10.3389/fmicb.2022.798685
16. Tsai CF, Chen GW, Chen YC, et al. Regulatory effects of quercetin on M1/M2 macrophage polarization and oxidative/antioxidative balance. *Nutrients*. 2021;14(1):67. doi:10.3390/nu14010067
17. Ni C, Zhou J, Kong N, et al. Gold nanoparticles modulate the crosstalk between macrophages and periodontal ligament cells for periodontitis treatment. *Biomaterials*. 2019;206:115–132. doi:10.1016/j.biomaterials.2019.03.039
18. Hussein H, Engineered Chitosan-based KA. Nanoparticles modulate macrophage-periodontal ligament fibroblast interactions in biofilm-mediated inflammation. *J Endod*. 2021;47(9):1435–1444. doi:10.1016/j.joen.2021.06.017
19. Shao J, Xie H, Huang H, et al. Biodegradable black phosphorus-based nanospheres for in vivo photothermal cancer therapy. *Nat Commun*. 2016;7:12967. doi:10.1038/ncomms12967
20. Chen W, Ouyang J, Liu H, et al. Black phosphorus nanosheet-based drug delivery system for synergistic photodynamic/photothermal/chemotherapy of cancer. *Adv Mater*. 2017;29:5.
21. Ding Q, Sun T, Su W, et al. Bioinspired multifunctional black phosphorus hydrogel with antibacterial and antioxidant properties: a stepwise countermeasure for diabetic skin wound healing. *Adv Healthc Mater*. 2022;11(12):e2102791. doi:10.1002/adhm.202102791
22. Qing Y, Li R, Li S, Li Y, Wang X, Qin Y. Advanced black phosphorus nanomaterials for bone regeneration. *Int J Nanomedicine*. 2020;15:2045–2058. doi:10.2147/IJN.S246336
23. Jeon S, Lee JH, Jang HJ, et al. Spontaneously promoted osteogenic differentiation of MC3T3-E1 preosteoblasts on ultrathin layers of black phosphorus. *Mater Sci Eng C Mater Biol Appl*. 2021;128:112309. doi:10.1016/j.msec.2021.112309
24. Qin L, Ling G, Peng F, et al. Black phosphorus nanosheets and gemcitabine encapsulated thermo-sensitive hydrogel for synergistic photothermal-chemotherapy. *J Colloid Interface Sci*. 2019;556:232–238. doi:10.1016/j.jcis.2019.08.058
25. Chambrone L, Wang HL, Romanos GE. Antimicrobial photodynamic therapy for the treatment of periodontitis and peri-implantitis: an American Academy of Periodontology best evidence review. *J Periodontol*. 2018;89(7):783–803. doi:10.1902/jop.2017.170172
26. Hou J, Wang H, Ge Z, et al. Treating acute kidney injury with antioxidative black phosphorus nanosheets. *Nano Lett*. 2020;20(2):14471454. doi:10.1021/acs.nanolett.9b05218
27. Hou YJ, Yang XX, Liu RQ, et al. Pathological mechanism of photodynamic therapy and photothermal therapy based on nanoparticles. *Int J Nanomedicine*. 2020;15:6827–6838. doi:10.2147/IJN.S269321
28. Wu K, Fu M, Zhao Y, et al. Anti-oxidant anti-inflammatory and antibacterial tannin-crosslinked citrate-based mussel-inspired bioadhesives facilitate scarless wound healing. *Bioact Mater*. 2022;20:93–110. doi:10.1016/j.bioactmat.2022.05.017
29. Mao L, Wang L, Zhang M, et al. In situ synthesized selenium nanoparticles-decorated bacterial cellulose/gelatin hydrogel with enhanced antibacterial, antioxidant, and anti-inflammatory capabilities for facilitating skin wound healing. *Adv Healthc Mater*. 2021;10(14):e2100402. doi:10.1002/adhm.202100402
30. Wang Y, Li C, Wan Y, et al. Nanocomposite potentiate dual-directional immunoregulation via macrophage polarization against periodontal inflammation. *Small*. 2021;17(41):e2101505. doi:10.1002/smll.202101505